Physics of the Earth and Planetary Interiors 283 (2018) 43–47

Contents lists available at ScienceDirect

Physics of the Earth and Planetary Interiors

journal homepage: www.elsevier.com/locate/pepi

The effect of nickel on the strength of iron nickel alloys: Implications for the Earth's inner core

Mary M. Reagan[a,*], Arianna E. Gleason[a,d], Jin Liu[a], Michael J. Krawczynski[b], James A. Van Orman[c], Wendy L. Mao[a,d]

[a] Department of Geological Sciences, 450 Serra Mall, Braun Hall, Building 320, Stanford University, Stanford, CA 94305, USA
[b] Department of Earth and Planetary Sciences, 1 Brookings Drive, Washington University, St. Louis, MO 63130, USA
[c] Department of Earth, Environmental and Planetary Sciences, Case Western Reserve University, 10900 Euclid Avenue, Cleveland, OH 44106, USA
[d] Stanford Institute for Materials and Energy Sciences, SLAC National Accelerator Laboratory, Menlo Park, CA 94025, USA

ARTICLE INFO

Keywords:
High pressure
Strength
Earth's inner core
Deformation
FeNi alloy

ABSTRACT

We investigated the effect of nickel on the strength of iron-nickel (FeNi) alloys at high pressure. Using radial X-ray diffraction coupled with literature results from nuclear resonance inelastic X-ray scattering measurements we determined the bulk strength of two FeNi alloys ($Fe_{0.88}Ni_{0.12}$ and $Fe_{0.8}Ni_{0.2}$) at high pressures up to 70 GPa. When extrapolated to Earth's inner core conditions, the strength of these FeNi alloys is found to increase relative to pure Fe. For the likely composition and conditions of the inner core, we estimate that an FeNi alloy with ~5.5 wt% Ni would have a strength that is ~125% greater than estimates for pure Fe. As shear strength is a measure of a material's resistance to flow, our results have implications for understanding the deformation processes inside planetary interiors and support dislocation creep as the dominant mechanism in the Earth's inner core.

1. Introduction

The Earth's inner core, located 5150–6370 km within the planet, is subjected to extreme pressure and temperature conditions that range from 330 to 364 GPa and ~4000–7000 K (Antonangeli, 2016). It is primarily composed of iron with 5–15% nickel, and a certain amount of light element(s) (Birch, 1952, 1964; Hirose et al., 2013). At inner core conditions, iron-rich FeNi alloys likely crystallize in an hexagonal close packed (hcp) phase (e.g., Lin et al., 2002; Liu et al., 2016; Mao et al., 2006; Tateno et al., 2010; Tateno et al., 2012; Sakai et al., 2011), although one recent theoretical study suggests that the stable phase may be body centered cubic (bcc) (Belonoshko et al., 2017). The Earth inner core exhibits a complex structure with seismic anisotropy, where seismic waves travel ~3% faster in the polar than the equatorial direction (Creager, 1992; Morelli et al., 1986; Shearer, 1994; Song and Helmberger, 1993; Tromp, 1993; Woodhouse et al., 1986), and lateral and hemispherical variations (Bréger et al., 2000; Cao and Romanowicz, 2004; Creager, 1999; Deuss et al., 2010; Irving, 2016; Song and Helmberger, 1995; Sun and Song, 2002; Vinnik et al., 1994). Gleason and Mao (2013) extrapolated the shear strength of pure iron to inner core conditions and determined it was weaker than previously thought, supporting that dislocation creep may be the dominant creep mechanism in the inner core. Pure Fe has been used as a proxy to understand the nature of the inner core including numerous studies on materials properties at high pressure and high temperature conditions (e.g. Struzhkin et al., 2004; Shen et al., 2004; Mao et al., 2008; Lin et al., 2005; Mao et al., 2001; Merkel et al., 2013; Tateno et al., 2010). There is a measured velocity-density profile discrepancy between the values of pure Fe and the those of the inner core, together with cosmochemical and geochemical observations, indicting the presence of Ni and other light elements (Birch, 1964), thus quantifying the effects of the addition of Ni on the geophysical properties of Fe is important. We examined the effect of varying nickel content on the strength of pure iron by studying $Fe_{0.88}Ni_{0.12}$ and $Fe_{0.8}Ni_{0.2}$ up to 70 GPa.

We define strength, t, as the maximum shear stress a material can withstand before undergoing plastic deformation. All values were calculated by anisotropic linear elasticity theory using the following methodology developed by Singh and Balasingh (1994) and Singh et al. (1998a,b). Non-hydrostatic pressure conditions produce lattice strains in a sample loaded into a diamond-anvil cell (DAC) that can be measured using radial X-ray diffraction, where the X-ray beam is nearly perpendicular to the compression axis. The geometry of a radial X-ray diffraction experiment is shown in Fig. 1. Samples in a DAC experience two stresses: axial stress, σ_3, and radial stress, σ_1. The deviatoric stress

* Corresponding author.
E-mail address: mreagan@stanford.edu (M.M. Reagan).

https://doi.org/10.1016/j.pepi.2018.08.003
Received 2 August 2017; Received in revised form 18 July 2018; Accepted 5 August 2018
Available online 06 August 2018

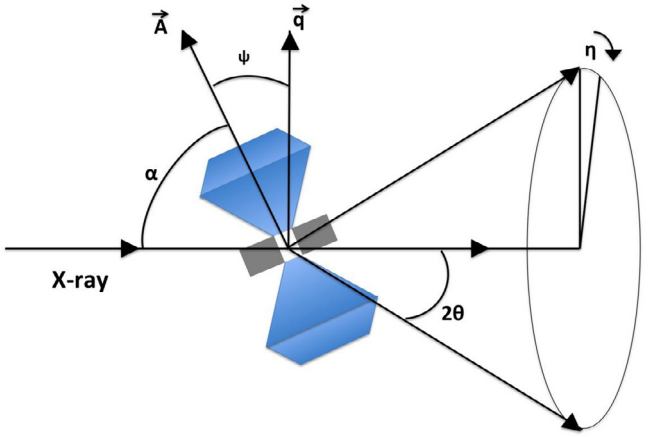

Fig. 1. Schematic for the setup of a radial diffraction experiment. The incident monochromatic X-ray beam is nearly perpendicular to the compression direction of a non-hydrostatically loaded DAC. *2θ* is the diffraction angle; *η* is the azimuth angle; *ψ* is the angle between the diamond compression axis and the momentum transfer; and *α* is the angle between the diamond compression axis and the X-ray beam.

component is given by $t = \sigma_3 - \sigma_1$, equivalent to the lower bound of the shear strength, which we refer to as *t*. Line shifts in the diffraction pattern provide a measure of the deviatoric strain relative to the hydrostatic strain for a crystallographic orientation and lattice plane. The *d*-spacing measured under non-hydrostatic compression, d_m (*hkl*), is given by

$$d_m(hlk) = d_p(hkl)[1 + (1-3cos^2\psi)\, Q\,(hkl)], \quad (1)$$

where d_p (*hkl*) is the *d*-spacing under hydrostatic condition, *ψ*, is the angle between the compression direction and the diffraction vector, and *Q* (*hkl*) is the differential strain. When $\psi = 54.7^\circ$ gives d_p (*hkl*), the *d* spacing equals that of hydrostatic conditions. Eq. (1) is valid for all crystal systems. The deviatoric strain produced by *d*(*hkl*) for a given *ψ* is given by

$$\varepsilon_\psi(hkl) = \frac{[d_\psi(hkl) - d_p(hkl)]}{d_p(hkl)} \quad (2)$$

A material's strength can be related to its shear modulus, *G*, and the average value of the differential strain, $< Q(hkl) >$, for all observed reflections by

$$t \approx 6G\langle Q(hkl)\rangle. \quad (3)$$

2. Methods

The $Fe_{0.88}Ni_{0.12}$ and $Fe_{0.8}Ni_{0.2}$ starting materials were synthesized with Fe and bbNi nanopowders, along with a small amount (1.7 vol%) of Si nanopowder (supplier, Alfa Aesar). Two different powder mixes were made, one with 80%Fe-20% Ni and the other with 88%Fe-12% Ni atomic abundances. The nanopowder mix was ultrasonicated in ethanol for several hours to mix thoroughly and dried in air. The powder mix was placed in a silica glass crucible, which was then inserted into a larger silica glass capsule. Between the inner crucible containing the sample and the outer capsule, we placed a powder consisting of a mixture of Fe with 1.6 wt% Si to ensure that the fO_2 remained below the IW buffer during the synthesis. The assembly was evacuated of air and sealed with an oxyacetylene torch. After sealing the outer capsule, it was placed in a 1 atm muffle furnace, heated to 1100 °C, and annealed for 3–4 days, then removed from the furnace and allowed to cool in air. Synthesized FeNi alloys were characterized by electron microprobe to ensure they were homogeneous.

Each sample was loaded into panoramic diamond anvil cells with 300 um flat culets in Be gaskets. Radial X-ray diffraction experiments were performed at Beamline 12.2.2 (λ = 0.4959 Å) of the Advanced Light Source (ALS), Lawrence Berkeley National Laboratory (LBNL), and at HP-CAT, beamline 16-BM-D (λ = 0.4133 Å) at the Advanced Photon Source (APS), Argonne National Laboratory (ANL). Pressure was determined using the equations of state for pure Fe (Dewaele et al., 2006) and $Fe_{0.8}Ni_{0.2}$ (Mao et al., 1990). Data analysis was performed using fit2D (Hammersley, 1998), with each diffraction image integrated over 10° azimuthal intervals. A sample slice of the integrated pattern is shown in Fig. 2a. The *d*-spacings for the hcp phase were determined for each slice and are seen to change as a function of azimuthal angle, η (Fig. 2b, d). Using equations (1) and (2), values of *Q*(*hkl*) are obtained from plotting *ε* (*hkl*) vs. $(1-3cos^2\psi)$. Strength was calculated using equation (3) where *G is* obtained from Lin (2003) for $Fe_{0.88}Ni_{0.12}$, and Kantor et al. (2007) for $Fe_{0.8}Ni_{0.2}$.

3. Results and discussion

Strength measurements were collected up to 47 GPa for $Fe_{0.88}Ni_{0.12}$ and 70 GPa for $Fe_{0.8}Ni_{0.2}$. $Fe_{0.88}Ni_{0.12}$ completed a transition to the hcp structure at 20 GPa and steadily increased in strength from 2.0 GPa to 2.8 GPa between 21 and 47 GPa. $Fe_{0.8}Ni_{0.2}$ made a complete transition to hcp at 35 GPa. Strength measurements were collected up to 70 GPa and are seen to increase from 1.6 to 4.2 GPa (Table 1). Fig. 3 shows a comparison of the different strength measurements for $Fe_{0.88}Ni_{0.12}$, $Fe_{0.8}Ni_{0.2}$, and hcp Fe (Gleason and Mao, 2013). We found that over the same pressure range (~20–50 GPa), the strength of $Fe_{0.88}Ni_{0.12}$ is approximately 6% higher than pure Fe, while the rate of increase in strength with increasing pressure for both materials is very similar. $Fe_{0.8}Ni_{0.2}$ starts at comparable strength values to pure Fe and $Fe_{0.88}Ni_{0.12}$ from 35 to 50 GPa, but increases in strength at higher pressures (54–70 GPa). At 65 GPa, $Fe_{0.8}Ni_{0.2}$ is stronger than pure Fe by ~25%. Reflecting this, $Fe_{0.8}Ni_{0.2}$'s *dt/dP* is larger at 0.066 than both $Fe_{0.88}Ni_{0.12}$ and Fe, whose values are 0.025 and 0.017 respectively.

We extrapolated our results to inner core pressures and temperatures using the Steinberg-Guinan model (Steinberg et al., 1980):

$$G(P, T) = G_0 + \frac{\partial G}{\partial P}\frac{P}{(\rho/\rho_0)^{1/3}} + \frac{\partial G}{\partial T}(T-300) \quad (4)$$

where ρ is density. First we solve for $\partial G/\partial T$ by setting *G* (*P*,*T*) and ρ to a range of Preliminary Reference Earth Model (PREM) values corresponding to outer most (P = 329 GPa) and center (*P* = 364 GPa) of the inner core where *G*(*P*,*T*) = 157 GPa or 176 GPa and *T* = 5500 and 6200 K respectively. G_0, $\partial G/\partial P$, and ρ_0 are experimental values taken from Lin (2003) and Kantor et al. (2007). High pressure and temperature *Q*(*hkl*) is taken from a linear extrapolation and used to calculate *t*. Fig. 4 shows the results of these extrapolations at fixed pressures of 329 GPa and 364 GPa from 3000 K to 6000 K. We find that with increasing nickel content at inner core conditions both compositions would likely exhibit higher strength than pure Fe. Increasing temperature decreases the strength for all compounds, decreasing the most for $Fe_{0.8}Ni_{0.2}$ and additionally diminishes the difference between them. A comparison for the estimated strength values at the center of the inner core are summarized in Table 2. We note that while we found that nickel can have a dramatic effect on the strength of iron over the pressure range we investigated, our extrapolation to inner core conditions requires assumptions about how our measured values will continue to change with increasing pressure and at high temperature, thus highlighting the need for future experiments at core conditions.

Our work supports the assertion that dislocation creep dominates the majority of the inner core. Creep is the tendency for a material to plastically deform when subjected to long-term exposure to differential stress and is therefore directly related to its strength. Plastic deformation can occur through a variety of mechanisms (Poirier, 1985), however all involve the motion of dislocations, point defects and grain boundaries. The common mechanisms thought to be operating within

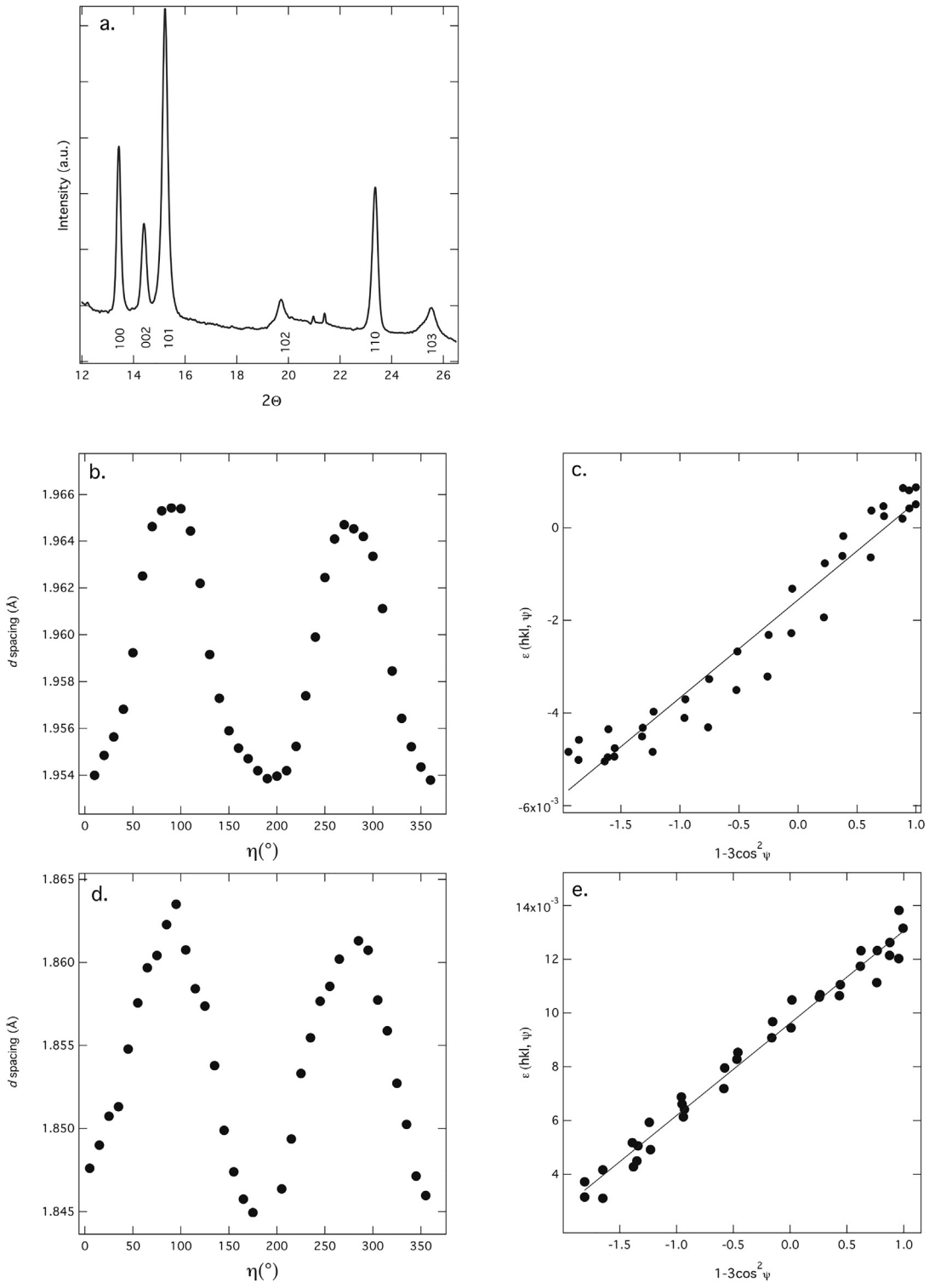

Fig. 2. a) A single integrated 10° slice of $Fe_{0.8}Ni_{0.2}$ diffraction pattern at 35 GPa; b) *d*-spacing as a function of azimuth angle for 100; c) deviatoric strain as a function of $1-3cos^2\psi$ for 100, where the slope gives the value of $Q(hkl)$. Error bars are smaller than the symbols; d) *d*-spacing as a function of azimuth angle for $Fe_{0.88}Ni_{0.12}$ at 29 GPa and 100; e) deviatoric strain as a function of $1-3cos^2\psi$ for 100, where the slope gives the value of $Q(hkl)$.

the core include: diffusion creep caused by stress-induced diffusion of atoms, dislocation creep caused by thermally activated motion of dislocations and grain boundary processes where deformation occurs mainly at grain boundaries (Merkel et al., 2016). According to Reaman et al. (2011) the very top of the inner core, where grain sizes are small, experiences diffusion creep, while the majority of the inner core, where increasing depth leads to increasing grain size and decreasing stress and strain rates, dislocation creep will dominate. Material strength will impact both mechanisms but will have an order of magnitude larger effect on dislocation mobility. Strength measurements can be related to the dislocation velocity through combining

$$v(\tau,T) = \frac{v_D a' b L}{w^2} \exp\left(\frac{-\Delta H_0}{kT}\right) \sinh\left(\frac{\Delta H_0 - \Delta H(\tau)}{kT}\right) \quad (5)$$

Table 1
Strength values for $Fe_{0.88}Ni_{0.12}$ and $Fe_{0.8}Ni_{0.2}$ at high pressure and ambient temperature.

Sample	Pressure (GPa)	Strength (GPa)
$Fe_{0.88}Ni_{0.12}$	21 (± 0.1)	2.0 (± 0.2)
	24 (± 0.1)	2.5 (± 0.5)
	29 (± 0.2)	2.6 (± 0.3)
	43 (± 0.3)	2.8 (± 0.5)
	47 (± 0.3)	2.8 (± 0.2)
$Fe_{0.8}Ni_{0.2}$	39 (± 0.4)	2.6 (± 0.8)
	43 (± 0.4)	2.4 (± 0.8)
	51 (± 0.5)	2.8 (± 0.3)
	53 (± 0.6)	3.0 (± 0.2)
	57 (± 0.5)	4.0 (± 0.8)
	60 (± 0.6)	4.1 (± 0.8)
	64 (± 0.7)	3.5 (± 0.5)
	69 (± 0.7)	4.2 (± 0.4)
	70 (± 0.7)	4.0 (± 0.3)

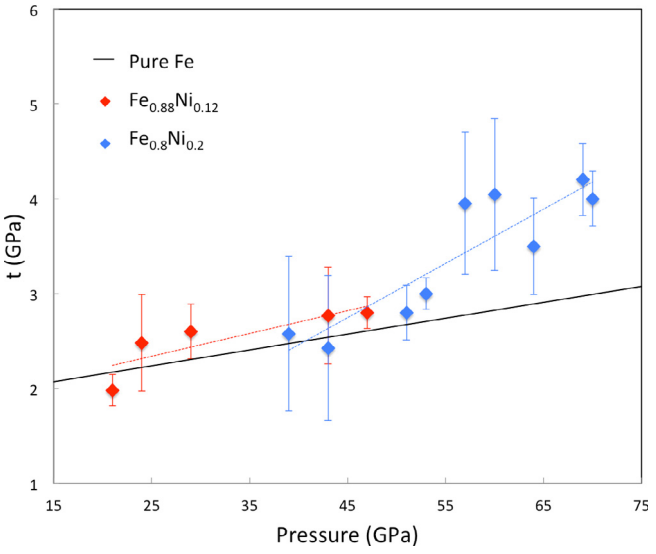

Fig. 3. A comparison of the strengths of pure Fe, $Fe_{0.88}Ni_{0.12}$, and $Fe_{0.8}Ni_{0.2}$ at high pressure and room temperature. Trend for pure Fe was calculated from Gleason and Mao, 2013 (black line). Dotted lines are linear fits for $Fe_{0.88}Ni_{0.12}$ (red) and $Fe_{0.8}Ni_{0.2}$ (blue). (For interpretation of the references to colour in this figure legend, the reader is referred to the web version of this article.)

and

$$\Delta H(\tau) = \Delta H_0[1-(\tau/\tau_p)^{3/4}]^{4/3} \quad (6)$$

where v(τ,T) is the dislocation velocity, v_D is the Debye frequency, a' is the Peierls barrier width, b is the Burgers vector, L Is the length of the dislocation, w is the width of kink pairs, τ is the applied stress, ΔH is the activation enthalpy, and k is the Boltzmann constant. τ_p is the Peierls stress, which measures the intrinsic lattice friction opposed to plastic shear (Nabarro, 2003, 2004). Setting τ_p equal to t, showing how dislocation velocity scales with strength, we find dislocation velocity rates for inner core conditions (τ_p = 2.4 GPa, 6200 K and 5500 K) that are between 10^{-4} m/s and 10^{-5} m/s, which are on the order of previous studies (Cordier et al., 2012; Gleason and Mao, 2013). The strength of the inner core may be higher than was previously reported by Gleason and Mao (2013), as we expect the strength of $Fe_{94.5}Ni_{5.5}$ to be higher than that of pure Fe, but still within the range to support dislocation creep as the dominant deformation mechanism.

Based on our experiments on the FeNi system we report a positive correlation with Ni content and strength. For a likely inner core composition of FeNi alloy with 5.5% Ni, extrapolating our results combined with our best ability to quantify uncertainty would give a strength of approximately 4 GPa at the conditions in the center of our planet (Fig. 5). This is ~125% greater than pure Fe at the same conditions. Future work should examine a wider variety of compositions (e.g. considering Ni with other light elements) to higher pressures and temperatures. While knowledge of the strength of FeNi alloys is not enough to fully constrain the inner core's rheology, our data suggests that increasing Ni content in hcp Fe increases the material's strength although most likely not enough to change the dominant deformation mechanism.

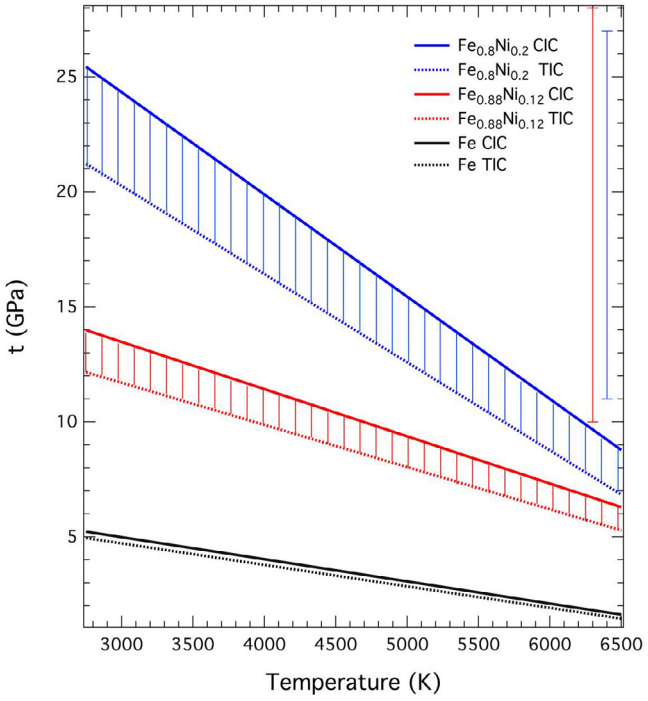

Fig. 4. Steinberg-Guinan temperature extrapolation (Steinberg et al., 1980) for pure Fe (Gleason and Mao, 2013), $Fe_{0.88}Ni_{0.12}$, and $Fe_{0.8}Ni_{0.2}$. Strength calculations were based on the center of the inner core (CIC); 364 GPa and 6200 K, to top of the inner core (TIC) conditions; 329 GPa and 6200 K. Representative uncertainties for both compositions at TIC pressure at 5500 K are shown at the top right.

Table 2
Strength and $\partial G/\partial T$ values for the top of the inner core (TIC, 329 GPa, 5500 K) and center of the inner core (CIC, 364 GPa, 6200 K) based on temperature extrapolation from Steinberg-Guinan model.

	TIC dG/dt	TIC Strength, t (GPa)	CIC dG/dt	CIC Strength, t (GPa)
Fe	−0.10	1.8	−0.09	1.6
$Fe_{0.88}Ni_{0.12}$	−0.06	5.7 (± 11.0)	−0.05	6.9 (± 11.8)
$Fe_{0.8}Ni_{0.2}$	−0.09	8.3 (± 10.1)	−0.08	10.1 (± 13.7)

Acknowledgements

M.M. Reagan, A.E. Gleason, and W.L. Mao are supported by the NSF Geophysics Program (EAR-1446969); and LANL LDRD for Gleason. M. J. Krawczynski was supported by NASA grant NNX15AJ25G. We thank Changyong Park (APS), Martin Kunz (ALS), and Jinyuan Yan (ALS) for their assistance with the synchrotron experiments. Portions of this work were performed at beamline 12.2.2 of ALS, LBNL. ALS is supported by the Director, Office of Science, Office of Basic Energy Sciences (BES), of the U.S. Department of Energy (DOE) under Contract No. DE-AC02-05CH11231. Portions of this work were also performed at HPCAT (Sector 16), APS, ANL. HPCAT operations are supported by DOE-NNSA

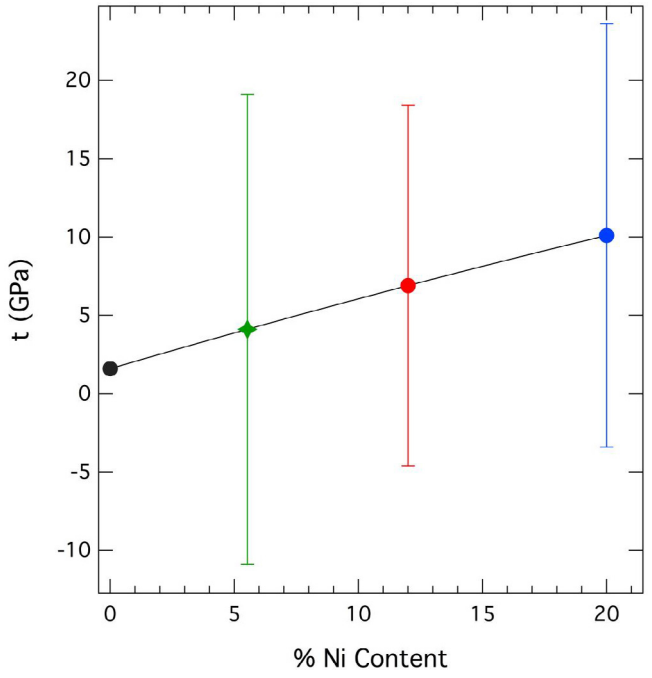

Fig. 5. Extrapolated strength values of hcp FeNi alloys with varying Ni content at center of the inner core (364 GPa, 6200 K) conditions. Values from Gleason and Mao (2013) (black circle) and this study (red and blue circles). Green star is the estimated value for a likely inner core composition of 5.5% Ni. (For interpretation of the references to colour in this figure legend, the reader is referred to the web version of this article.)

under Award No. DE-NA0001974 and DOE-BES under Award No. DE-FG02-99ER45775, with partial instrumentation funding by NSF. APS is a DOE-BES User Facility operated for the DOE Office of Science by ANL under Contract No. DE-AC02-06CH11357.

References

Antonangeli, D., 2016. Physical properties of the inner core. Deep Earth: Physics and Chemistry of the Lower Mantle and Core, (217th ed.).
Belonoshko, A.B., Lukinov, T., Fu, J., Zhao, J., Davis, S., Simak, S.I., 2017. Stabilization of body-centred cubic iron under inner-core conditions. Nat. Geosci. 10. https://doi.org/10.1038/ngeo2892.
Birch, F., 1952. Elasticity and constitution of the Earth's interior. J. Geophys. Res. 57 (2), 227–286. https://doi.org/10.1029/JZ057i002p00227.
Birch, F., 1964. Density and composition of mantle and core. J. Geophys. Res. 69 (20), 4377–4388. https://doi.org/10.1029/JZ069i020p04377.
Bréger, L., Tkalčić, H., Romanowicz, B., 2000. The effect of D″ on PKP(AB − DF) travel time residuals and possible implications for inner core structure. Earth Planet. Sci. Lett. 175 (1–2), 133–143. https://doi.org/10.1016/S0012-821X(99), 00286-1.
Cao, A., Romanowicz, B., 2004. Hemispherical transition of seismic attenuation at the top of the earth's inner core. Earth Planet. Sci. Lett. 228 (3–4), 243–253. https://doi.org/10.1016/j.epsl.2004.09.032.
Cordier, P., Amodeo, J., Carrez, P., 2012. Modelling the rheology of MgO under Earth's mantle pressure, temperature and strain rates. Nature 481 (7380), 177–180. https://doi.org/10.1038/nature10687.
Creager, K.C., 1992. Anisotropy of the inner core from differential travel times of the phases PKP and PKIKP. Nature 356 (6367), 309–314. https://doi.org/10.1038/356309a0.
Creager, K.C., 1999. Large-scale variations in inner core anisotropy. J. Geophys. Res. Solid Earth 104 (B10), 23127–23139. https://doi.org/10.1029/1999JB900162.
Deuss, A., Irving, J.C.E., Woodhouse, J.H., 2010. Regional variation of inner core anisotropy from seismic normal mode observations. Science 328 (5981), 1018–1020. https://doi.org/10.1126/science.1188596.
Dewaele, A., Loubeyre, P., Occelli, F., Mezouar, M., Dorogokupets, P.I., Torrent, M., 2006. Quasihydrostatic equation of state of Iron above 2 Mbar. Phys. Rev. Lett. 97 (21), 29–32. https://doi.org/10.1103/PhysRevLett. 97.215504.
Gleason, A.E., Mao, W.L., 2013. Strength of iron at core pressures and evidence for a weak Earth's inner core. Nat. Geosci. 6 (7), 571–574. https://doi.org/10.1038/ngeo1808.
Hammersley, A.P., 1998. Fit2D: V99.129.
Hirose, K., Labrosse, S., Hernlund, J., 2013. Composition and state of the core. Annu. Rev. Earth Planet. Sci. 41 (1), 657–691. https://doi.org/10.1146/annurev-earth-050212-124007.
Irving, J.C.E., 2016. Imaging the inner core under Africa and Europe. Phys. Earth Planet. Inter. 254, 12–24. https://doi.org/10.1016/j.pepi.2016.03.001.
Kantor, A.P., Kantor, I.Y., Kurnosov, A.V., Kuznetsov, A.Y., Dubrovinskaia, N.A., Krisch, M., Dubrovinsky, L.S., 2007. Sound wave velocities of fcc Fe-Ni alloy at high pressure and temperature by mean of inelastic X-ray scattering. Phys. Earth Planet. Inter. 164 (1–2), 83–89. https://doi.org/10.1016/j.pepi.2007.06.006.
Lin, J.-F., 2003. Sound velocities of iron-nickel and iron-silicon alloys at high pressures. Geophys. Res. Lett. 30 (21), 2112. https://doi.org/10.1029/2003GL018405.
Lin, J.-F., Heinz, D.L., Campbell, A.J., Devine, J.M., Mao, W.L., Shen, G., 2002. Iron-nickel alloy in the Earth's core. Geophys. Res. Lett. 29 (10). https://doi.org/10.1029/2002GL015089. 109-1-109–3.
Lin, J., Sturhahn, W., Zhao, J., Shen, G., Mao, H., Hemley, R.J., 2005. Sound velocities of hot dense iron: Birch's law revisited. Science 2563, 1892–1894.
Liu, J., Lin, J.F., Alatas, A., Hu, M.Y., Zhao, J., Dubrovinsky, L., 2016. Seismic parameters of hcp-Fe alloyed with Ni and Si in the Earth's inner core. J. Geophys. Res. Solid Earth 121, 610–623. https://doi.org/10.1002/2015JB012625.
Mao, W.L., Struzhkin, V.V., Baron, A.Q.R., Tsutsui, S., Tommaseo, C.E., Wenk, H.-R., Mao, H.-K., 2008. Experimental determination of the elasticity of iron at high pressure. J. Geophys. Res. 113 (B9), B09213. https://doi.org/10.1029/2007JB005229.
Mao, H.K., Wu, Y., Chen, L.C., Shu, J.F., 1990b. Static compression of iron to 300 GPa and Fe(0.8)Ni(0.2) alloy to 260 GPa – implications for composition of the core. J. Geophys. Res. 95 (B13), 21737. https://doi.org/10.1029/JB095iB13p21737.
Mao, H.K., Wu, Y., Chen, L.C., Shu, J.F., Jephcoat, P., 1990a. Static compression of iron to 300 GPa and FeNi20 alloy to 260 GPa: implication for composition of the core. J. Geophys. Res. 95 (90), 737–742.
Mao, H.K., Xu, J., Struzhkin, V.V., Shu, J., Hemley, R.J., Sturhahn, W., Wortmann, G., 2001. Phonon density of states of iron up to 153 gigapascals. Science 292 (5518), 914–916. https://doi.org/10.1126/science.1057670.
Merkel, S., Liermann, H.-P., Miyagi, L., Wenk, H.R., 2013. In situ radial X-ray diffraction study of texture and stress during phase transformations in bcc-, fcc- and hcp-iron up to 36GPa and 1000K. Acta Mater. 61 (14), 5144–5151. https://doi.org/10.1016/j.actamat.2013.04.068.
Morelli, A., Dziewonski, A.M., Woodhouse, J.H., 1986. Anisotropy of the inner core inferred from PKIKP travel times. Geophys. Res. Lett. 13 (13), 1545–1548. https://doi.org/10.1029/GL013i013p01545.
Nabarro, F.R.N., 2003. One-dimensional models of thermal activation under shear stress. Phil. Mag. 83 (26), 3047–3054. https://doi.org/10.1080/0141861031000109591.
F.R.N. Nabarro, Do we have an acceptable model of power-law creep? Mater. Sci. Eng. A, 387–389(1–2 SPEC. ISS.) (2004) 659–664. doi: 10.1016/j.msea.2003.09.118.
Sakai, T., Ohtani, E., Hirao, N., Ohishi, Y., 2011. Stability field of the hcp-structure for Fe, Fe-Ni, and Fe-Ni-Si alloys up to 3 Mbar. Geophys. Res. Lett. 38 (9). https://doi.org/10.1029/2011GL047178.
Shearer, P.M., 1994. Constraints on inner core anisotropy from PKP(DF) travel times. J. Geophys. Res. Solid Earth 99 (B10), 19647–19659. https://doi.org/10.1029/94JB01470.
Shen, G., Sturhahn, W., Alph, E.E., Zhao, J., Tollenner, T.S., Prakapenka, V.B., Mao, H.R., 2004. Phonon density of states in iron at high pressures and high temperatures. Phys. Chem. Miner. 31 (6), 353–359. https://doi.org/10.1007/s00269-004-0403-l.
Singh, A.K., Balasingh, C., 1994. The lattice strains in a specimen (hexagonal system) compressed nonhydrostatically in an opposed anvil high pressure setup. J. Appl. Phys. 75 (10), 4956–4962. https://doi.org/10.1063/1.355786.
Singh, A.K., Balasingh, C., Mao, H., Hemley, R.J., Shu, J., 1998a. Analysis of lattice strains measured under nonhydrostatic pressure. J. Appl. Phys. 83 (12), 7567. https://doi.org/10.1063/1.367872.
Singh, A., Mao, H., Shu, J., Hemley, R., 1998b. Estimation of single-crystal elastic moduli from polycrystalline X-ray diffraction at high pressure: application to FeO and iron. Phys. Rev. Lett. 80 (10), 2157–2160. https://doi.org/10.1103/PhysRevLett. 80.2157.
Song, X., Helmberger, D.V., 1993. Anisotropy of Earth's inner core. Geophys. Res. Lett. 20 (23), 2591–2594. https://doi.org/10.1029/93GL02812.
Song, X., Helmberger, D.V., 1995. Depth dependence of anisotropy of Earth's inner core. J. Geophys. Res.: Solid Earth 100 (B6), 9805–9816. https://doi.org/10.1029/95JB00244.
Steinberg, D.J., Cochran, S.G., Guinan, M.W., 1980. A constitutive model for metals applicable at high-strain rate. J. Appl. Phys. 51 (3), 1498–1504. https://doi.org/10.1063/1.327799.
Struzhkin, V.V., Mao, H., Mao, W.L., Hemley, R.J., Sturhahn, W., Alp, E.E., Errandonea, D., 2004. Phonon density of states and elastic properties of Fe-based materials under compression. Hyperfine Interact. 153 (1–4), 3–15. https://doi.org/10.1023/B:HYPE.0000024709.22242.57.
Sun, X., Song, X., 2002. PKP travel times at near antipodal distances: implications for inner core anisotropy and lowermost mantle structure. Earth Planet. Sci. Lett. 199 (3–4), 429–445. https://doi.org/10.1016/S0012-821X(02)00580-0.
Tateno, S., Hirose, K., Komabayashi, T., Ozawa, H., Ohishi, Y., 2012. The structure of Fe-Ni alloy in Earth's inner core. Geophys. Res. Lett. 39 (12). https://doi.org/10.1029/2012GL052103.
Tateno, S., Hirose, K., Ohishi, Y., Tatsumi, Y., 2010. The structure of iron in Earth's inner core. Science (New York, N.Y.) 330 (6002), 359–361. https://doi.org/10.1126/science.1194662.
Tromp, J., 1993. Support for anisotropy of the Earth's inner core from free oscillations. Nature 366 (6456), 678–681. https://doi.org/10.1038/366678a0.
Vinnik, L., Romanowicz, B., Breger, L., 1994. Anisotropy in the center of the inner core. Geophys. Res. Lett. 21 (16), 1671–1674. https://doi.org/10.1029/94GL01600.
Woodhouse, J.H., Giardini, D., Li, X.-D., 1986. Evidence for inner core anisotropy from free oscillations. Geophys. Res. Lett. 13 (13), 1549–1552. https://doi.org/10.1029/GL013i013p01549.